J Supercond Nov Magn (2016) 29:2881–2886
DOI 10.1007/s10948-016-3607-y

ORIGINAL PAPER

Investigation of Microwave Absorptive Behavior of La-Na Substituted M-Type Co-Zr Barium Hexaferrites in X-Band

Amit Arora[1] · **Sukhleen Bindra Narang**[2]

Received: 10 April 2016 / Accepted: 30 June 2016 / Published online: 19 July 2016

Abstract La-Na-substituted Co-Zr barium hexaferrites were fabricated using the conventional ceramic sintering method. Characterization techniques like X-ray diffraction (XRD), scanning electron microscopy (SEM), vibration sample magnetometry (VSM) and vector network analysis (VNA) were used to analyze structural, magnetic and microwave absorption properties of prepared ferrites. The results show that the magnetoplumbite structures for all the samples have been formed. The magnetic properties such as saturation magnetization (M_s), remanence (M_r) and coercivity (H_c) were calculated from hysteresis loops obtained using a vibrating sample magnetometer (VSM). Also the present investigation demonstrates that microwave absorber using $Ba_{(1-2x)}La_xNa_xFe_{10}CoZrO_{19}$ ferrite can be fabricated for the applications in frequency band from 8.2 to 12.4 GHz, with a reflection loss less than −10 dB for specific frequencies, by controlling the molar ratio of the substituted ions.

Keywords Barium hexaferrite · Dielectric properties · Reflection loss · Microwave absorber

✉ Sukhleen Bindra Narang
sukhleen2@yahoo.com

[1] DAV Institute of Engineering and Technology, Jalandhar, India

[2] Department of Electronics Technology, Guru Nanak Dev University, Amritsar, India

1 Introduction

With the development of radar and microwave communication technology, there is a need for anti-electromagnetic interference devices in order to minimize electromagnetic reflection from large structures such as aircrafts, ships, and tanks (stealth technology). For this reason, electromagnetic wave-absorbing materials with the capability of absorbing unwanted electromagnetic signals have become one of the most crucial high-tech materials in recent years [1–4]. Ferrites are considered to be the best magnetic material for electromagnetic wave absorbers due to their excellent magnetic and dielectric properties. Spinel ferrites and metallic magnetic materials have been used as conventional microwave absorption materials. However, the usage of spinel ferrites is limited to low frequencies due to Snoek's limit as their magnetic loss drastically decreases at higher frequencies [5, 6]. Metallic magnetic materials show high permeability, but they are required to be insulated to prevent eddy current losses [7, 8]. Among all the ferrites, barium ferrites with hexagonal magnetoplumbite structure have been considerably studied as one of the most important microwave-absorbing materials because of their high coercive force, large magnetocrystalline anisotropy, high saturation magnetization, excellent chemical stability and corrosion resistivity [9, 10]. A lot of research work has been done in the field of hexaferrites but the work always remained short of electromagnetic and absorption characterization [11, 12]. In this study, we have presented a detailed microwave characterization of co-substituted M-type barium hexaferrites along with their magnetic properties.

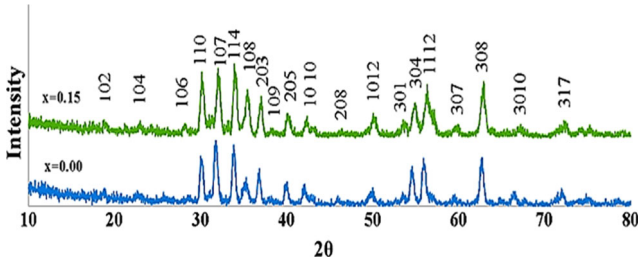

Fig. 1 X-ray diffraction patterns of $Ba_{(1-2x)}La_xNa_xFe_{10}CoZrO_{19}$ ($x = 0.00, 0.15$)

2 Experimental Procedure

2.1 Preparation of Samples

The synthesis of the hexaferrite compound with chemical formula $Ba_{(1-2x)}La_xNa_xFe_{10}CoZrO_{19}$ (with $x = 0.0$, 0.05, 0.10, 0.15, 0.20, 0.25) was done using the high-temperature solid-state reaction technique [13, 14]. The preparation method and detailed structural analysis of this series have already been published [15]. The calcination of the samples was performed at 1250 °C for 8 h and sintering of the samples was done at 1250 °C for 3 h.

2.2 Measurement of Properties

The crystalline phases in the prepared samples were examined by XRD spectroscopy by employing an X-ray diffractometer (Brukers D8 Focus) and the diffraction points were recorded from 10° to 80°. Microstructural analysis of the prepared samples was performed by a scanning electron microscope (Zeiss-Supra 55). The magnetic properties of the samples were investigated at room temperature using a Microsense EZ9 vibrating sample magnetometer (VSM). The evaluation of the microwave absorption properties was studied by using the Agilent N5225A Vector Network Analyzer (VNA). The variation of the complex permittivity, complex permeability and reflection loss (in decibels) versus frequency in the range of 8.2–12.4 GHz has been investigated.

3 Results and Discussion

3.1 Phase Identification

The XRD diffraction patterns of $Ba_{(1-2x)}La_xNa_xFe_{10}CoZrO_{19}$ ($x = 0.0$, 0.15) ferrite samples, obtained using Cu-Kα radiation are shown in Fig. 1. The peaks for the doped barium ferrite appear at the same position as the undoped ferrite, but with different intensity that corresponds to the space group P63/mmc(194) referred from standard JCPDS data file no. 078-0131.

3.2 SEM Microstructures

The microstructures of the formed samples of the prepared ferrites calcined at 1250 °C are shown in Fig. 2. The surface morphology of the samples indicates that the prepared ferrite samples have the average grain size between 250 and 380 nm [16–18].

3.3 Magnetic Properties

The magnetic properties have been investigated as a function of substitution of La^{3+} and Na^{+} ions at applied fields of −20 to +20 kOe. The hysteresis loops of the prepared $Ba_{(1-2x)}La_xNa_xFe_{10}CoZrO_{19}$ solid solutions for $0.00 \leq x \leq 0.25$ are shown in Fig. 3. It is observed that for all compositions, there is an abrupt rise in the magnetization at a low applied field followed by slow variation at a high applied field. The values of the saturation magnetization (M_s), coercivity (H_c), remanence (M_r) and magnetocrystalline anisotropy (H_a) were obtained from hysteresis loop data and are shown in Table 1. The saturation magnetization (M_s) decreases with an increase in substitution from

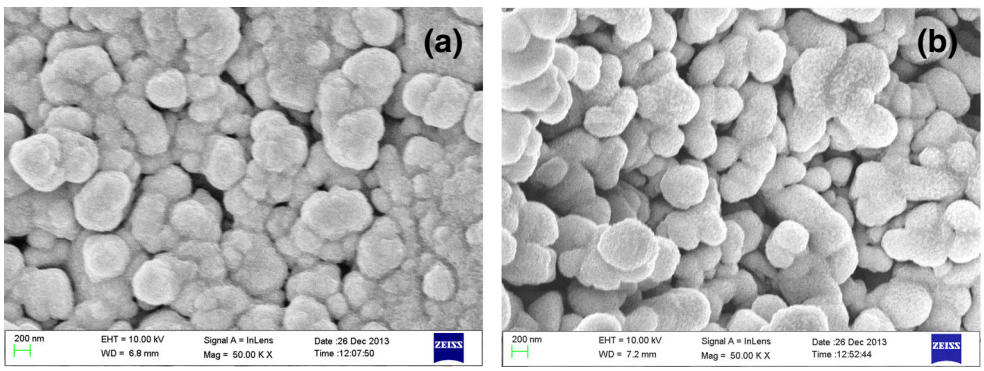

Fig. 2 SEM images of $Ba_{(1-2x)}La_xNa_xFe_{10}CoZrO_{19}$. **a** $x = 0.00$, **b** $x = 0.15$

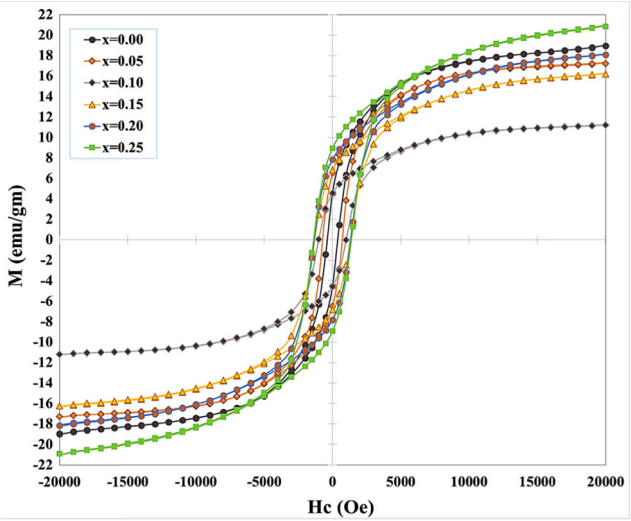

Fig. 3 Hysteresis loops of $Ba_{(1-2x)}La_xNa_xFe_{10}CoZrO_{19}$ samples for different substitution (x) at room temperature

18.95 emu/g for $x = 0.00$ to 11.18 emu/g for $x = 0.10$ and then increases to 20.91 emu/g for $x = 0.25$. The elementary unit cell of M-type hexagonal ferrite contains ten oxygen layers, constructed sequentially from four blocks: S (spinel), R (hexagonal), S* and R*. The S* and R* blocks have equivalent atomic arrangements but are rotated at 180° with respect to the S and R blocks around the c-axis. The S or S* blocks consist of two O^{2-} layers and the R or R* blocks contain three O^{2-} layers, with one oxygen site in the middle layer substituted by a Ba^{2+} ion. There are 64 ions per unit cell on 11 sites of different symmetry. Twenty-four Fe^{3+} ions are distributed over five distinct sites: three octahedral sites (12k, 2a and 4f2), one tetrahedral site (4f1) and one bipyramidal site (2b). The Gorter model suggests a ferrimagnetic structure comprising three parallel (4f1 and 4f2) and eight antiparallel (12k, 2a and 2b) spins which are coupled by superexchange interactions through the O^{2-} ions. The magnetic moment of the hexaferrite samples is determined from the sum of magnetic moments of ions at different positions in different crystal interstitial sites [19–21].

$$M = M[(12k \uparrow + 2b \uparrow + 2a \uparrow) - (4f2 \downarrow + 4f1 \downarrow)]$$

As shown in Table 1, the decrease in saturation magnetization (M_s) with the increase in substitution might be due to the increase in non-magnetic La^{3+} and Na^{+} ions giving dilution of the internal magnetic field and weakening of the Fe^{3+}-O-Fe^{3+} super-exchange interaction. For $x > 0.10$ the value of M_s increases, which might be due to occupancy of spin-down lattice sites $4f_1$ and $4f_2$ by non-magnetic La^{3+} and Na^{+} ions. The trend of Curie temperature (T_C) variation is similar to that of M_s, which first decreases and then increases with an increase in substitution of La-Na. It is expected also as when M_s increases, more energy is required to offset its effect, which is in accordance with the observed values of M_s and T_C for the prepared samples. Coercivity (H_c) is found to increase with an increasing substitution level, which might be due to the increase in magnetocrystalline anisotropy (H_a) and the decrease in the unit cell volume because of a smaller size of La^{3+} (1.13 Å) and Na^{+} (1.02 Å) ions as compared to the size of the Ba^{2+} (1.34 Å) ion. There is wide variation in coercivity in the prepared samples from 380.52 to 374.79 Oe. Coercivity depends inversely on grain size and directly on magnetocrystalline anisotropy [22]. The variation of saturation magnetization (M_s) and coercivity (H_c) versus substitution amount (x) for the samples is shown in Fig. 4.

Our results show that the magnetic properties are closely related to the distribution of La-Na ions in the lattice structure of the crystal. It is observed that in coupled substitution of ferrites the tendency to occupy a particular site is an interplay of several factors like the difference in electronegativities and ionic radii of the dopants.

3.4 Electromagnetic and Absorption Characteristics

The absorption characteristic of the undoped barium hexaferrite is in the higher-frequency range (around 45 GHz) and its bandwidth is too small to be used as microwave absorption material [23, 24]. Therefore, doping of La-Na has been done in Co-Zr-substituted barium hexaferrites in order to improve its absorption characteristics. The complex scattering parameters that correspond to the reflection (S_{11} or S_{22}) and transmission (S_{21} or S_{12}) in the prepared samples were measured using a vector network analyzer. Full two-port

Table 1 Values of the M_s, H_c, M_r, and H_a for different substitution (x) of La-Na-substituted samples

Sample (x)	M_s (emu/g)	H_c (Oe)	M_r (emu/g)	H_a (Oe)	Curie temperature (°C)
0.00	18.95	380.52	4.55	384.02	662
0.05	17.28	715.46	6.51	274.25	468
0.10	11.18	1006.69	4.55	297.81	506
0.15	16.26	1297.73	6.82	344.74	536
0.20	18.12	1326.08	7.83	356.91	580
0.25	20.91	1374.80	8.94	415.83	652

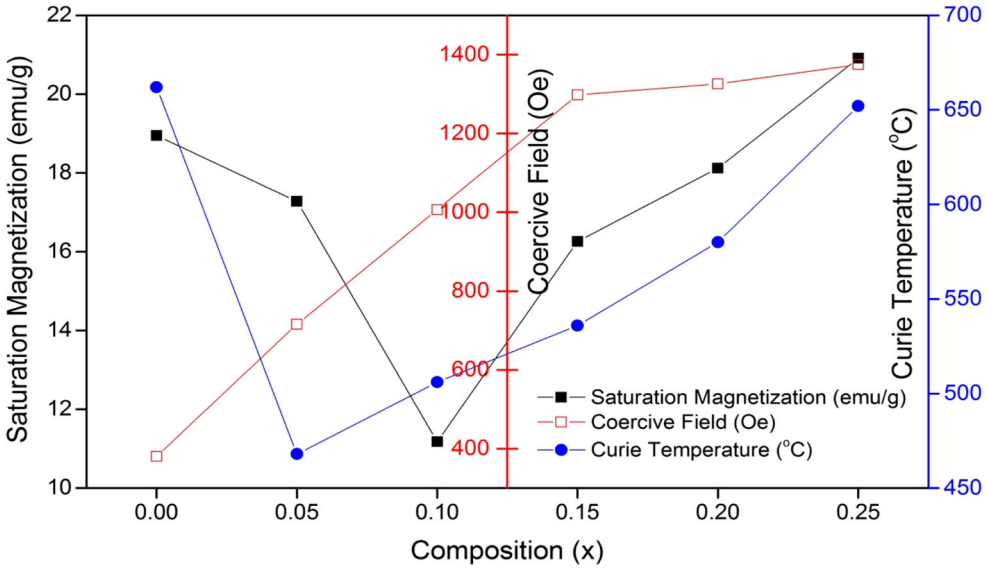

Fig. 4 M_s, H_c, and T_C dependence on the substitution (x) for $Ba_{(1-2x)}La_xNa_xFe_{10}CoZrO_{19}$ samples

calibrations were initially done on the test setup in order to remove the errors due to the directivity, source match, load match, isolation, etc. The complex permittivity and permeability were then determined from the measured scattering parameters using Agilent software module 85071.

The reflection loss (RL) is related to the normalized input impedance (Z_{in}) of a metal-backed microwave-absorbing layer as

$$\mathrm{RL\,(db)} = 20\log\left|\frac{Z_n - 1}{Z_n + 1}\right| \quad \text{and} \quad Z_n = \sqrt{\frac{\mu_r}{\epsilon_r}}\tanh\left[j\frac{2\pi f d\sqrt{\mu_r\epsilon_r}}{c}\right]$$

where μ_r and ε_r are the complex relative permeability and complex relative permittivity of the synthesized samples respectively, c is the velocity of light in free space, f is the frequency and d is the thickness of the absorber [25–27]. Figure 5 shows the permittivity/dielectric constant and dielectric loss and Fig. 6 shows the permeability and magnetic loss of the prepared samples in X-band frequencies. The net loss tangent comprising dielectric and magnetic loss tangents is shown in Fig. 7. Reflection loss is calculated using the measured values of complex permittivity and complex permeability and is presented in Fig. 8.

As shown in Fig. 5, the dielectric constant (ε') of all the samples is between the range 6.5–10 and remains almost constant for each sample (very small variation with frequency), but it decreases as the substitution level is increased, which is due to the decrease in conductivity of the samples with substitution, as ε' is dependent on conductivity.

The dielectric loss of all the samples has remained in the range 0.6–0.32 for most of the frequency range. All the samples have observed peaks in the loss spectra after 11.2 GHz. The sample $x = 0.10$ has observed the maximum peak of 1.3 at 12 GHz frequency. There is an overall increasing trend of dielectric loss w.r.t. frequency for all the samples. It can be seen from Fig. 5 that dielectric losses have decreased as the value of substitution (x) is increased. This decreasing trend is very similar to that of the dielectric constant because the governing factor—polarization—is the same for both properties.

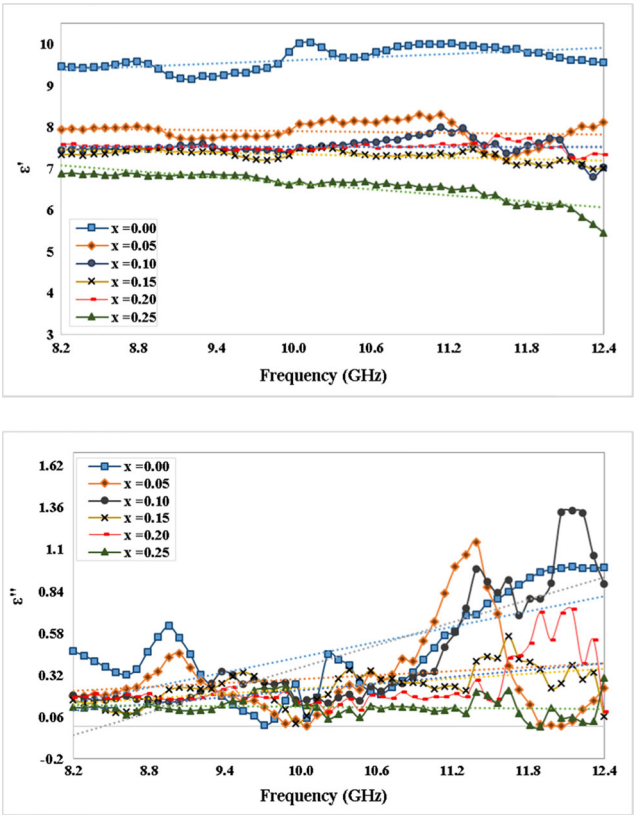

Fig. 5 Variation of dielectric constant (ε') and dielectric loss (ε'') with frequency for the samples $Ba_{(1-2x)}La_xNa_xFe_{10}CoZrO_{19}$

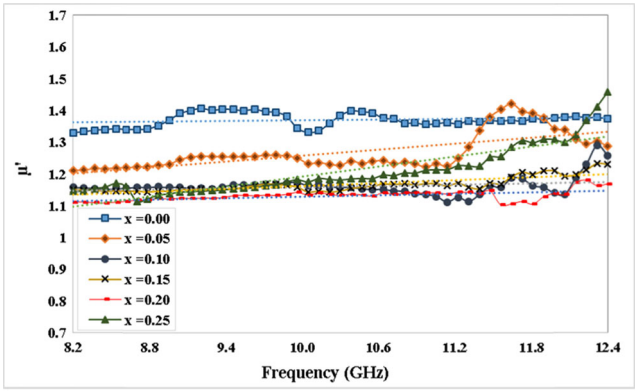

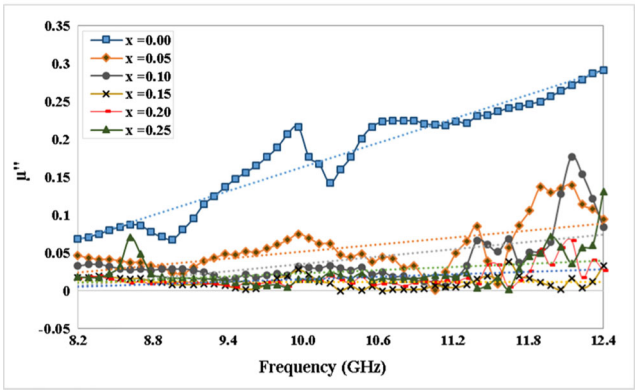

Fig. 6 Variation of permeability (μ') and magnetic loss (μ') with frequency for the samples $Ba_{(1-2x)}La_xNa_xFe_{10}CoZrO_{19}$

From Fig. 6, it is clear that the real part of permeability (μ') shows a decrease with an increase in substitution for all the samples, which may be due to the increase in porosity and grain boundaries of the samples with substitution. This causes a high reluctance to magnetic domain motion, thereby decreasing μ' and μ''. The magnetic loss arises due to a lag between the magnetization and applied field. The permeability μ' and magnetic loss μ'' remain almost constant w.r.t. frequency within the ranges 1.1–1.4 and 0.0–0.2 for the La-Na-doped samples.

According to the ferromagnetic theory, the imaginary part μ'' of complex permeability is affected by saturation magnetization, the anisotropy field and the extinction coefficient (α) and is given by the equation $\mu'' = M_s/2H_a\alpha$. The strong spin-orbit interaction of rare earth ions generates a high anisotropy field. Subsequently, the anisotropy field of the La-Na-substituted ferrites increases with substitution, which agrees well with the H_a results in Table 1. So, μ'' decreases according to the above equation with substitution [28].

Figure 7 shows the gross loss tangent; it indicates that the maximum value of the gross loss tangent is about 0.4 in the frequency of about 12.1 GHz for the sample $x = 0.10$. It may be caused by domain-wall displacement and lagging of domain rotation behind the applied magnetic field.

Reflection loss (RL) values are taken for the sample thickness 1.3 mm in the X-band frequency range (8.2–12.4 GHz) for the prepared samples. The reflection loss variation with frequency is shown in Fig. 6. For the sample $x = 0.0$, the reflection loss peak of −20 dB is observed at 11.14 GHz. The reflection loss peak for the sample $x = 0.05$ is observed to be −16.05 dB at 12.23 GHz. The matching frequency for the ferrite sample $x = 0.10$ is 11.89 GHz with a reflection loss of −30.28 dB. For sample $x = 0.15$, the value of reflection loss is −21.59 dB at 12.32 GHz. For sample $x = 0.20$, the reflection loss of −10.13 dB is observed at a frequency of 12.06 GHz, which is minimum among all the samples. For sample $x = 0.25$, the value of RL is −14.52 dB at 12.23 GHz. The reflection loss shows oscillatory behavior for the synthesized series with an increase in concentration of lanthanumsodium in $BaFe_{10}CoZrO_{19}$ hexaferrite. The reflection loss occurs due to absorption, destructive interference and multiple internal

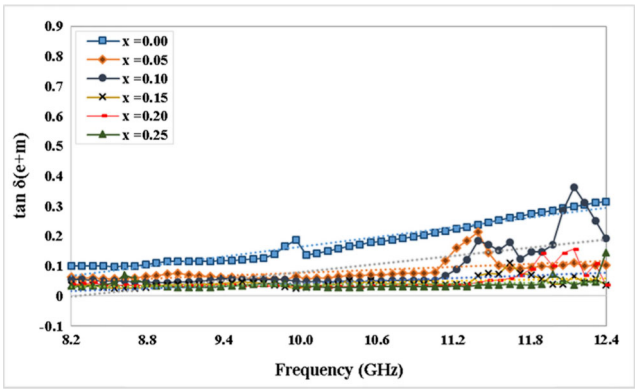

Fig. 7 Variation of gross loss tangent $\tan\delta_{(e+m)}$ with frequency for the samples $Ba_{(1-2x)}La_xNa_xFe_{10}CoZrO_{19}$

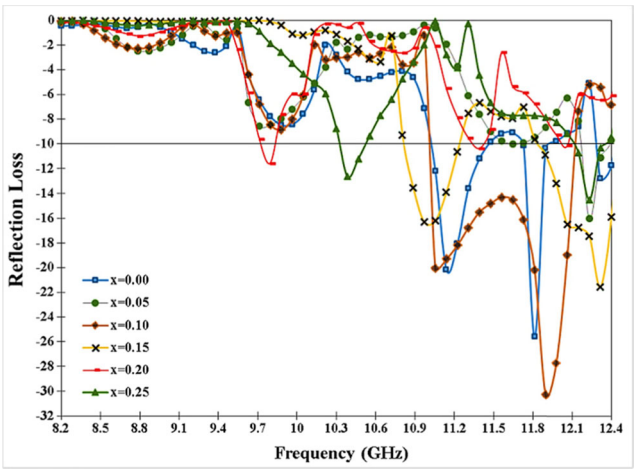

Fig. 8 Variation of reflection loss with frequency for the samples $Ba_{(1-2x)}La_xNa_xFe_{10}CoZrO_{19}$

reflections in the sample. All these phenomena are coupled together to result in a final reflection loss.

4 Conclusion

$Ba_{(1-2x)}La_xNa_xFe_{10}CoZrO_{19}$ hexaferrites are prepared by the solid-state reaction technique. Magnetic hysteresis loops of the samples show significant variation in the magnetic parameters which make these ferrites suitable for digital recording media. Doping of La-Na has resulted in the lowering of real permittivity and real permeability which makes them appropriate for impedance matching. From microwave absorption analysis of 1.3mmthick ferrite pellets in X-band, the conclusion can be drawn that practical absorbers can be obtained from these materials by controlling the substitution value of La-Na in Co-Zr-substituted barium hexaferrites, whose frequency of peak reflection loss is tunable depending on the amount of substitution. The $Ba_{0.8}La_{0.10}Na_{0.10}Fe_{10}CoZrO_{19}$ ferrite composition provides the best results in the prepared ferrite series and hence proves its potential for usage in practical applications in the 8.2–12.4 GHz frequency range.

References

1. Meshram, M.R., Agrawal, N.K., Sinha, B., Misra, P.S.: J. Magn. Magn. Mater. **271**(2–3), 207–214 (2004)
2. Roberto, D.A., Lima, C., Pinho, M.S., Gregori, M.L., Nunes, R.C.R., Ogasawara, T.: Mater. Sci. **22**(3) (2004)
3. Gairola, S.P., Verma, V., Singh, A., Purohit, L.P., Kotnala, R.K.: Solid State Commun. **150**(3–4), 147–151 (2010)
4. Narang, S.B., Chawala, S.K., Mudsainiyan, R.K., Pubby, K.: Integrated Ferroelectr. **167**(1), 98–106 (2015)
5. Ghasemi, A., Hossienpour, A., Morisako, A., Saatchi, A., Salehi, M.: J. Magn. Magn. Mater. **302**(2), 429–435 (2006)
6. Narang, S.B., Kaur, P., Bahel, S., Singh, C.: J. Magn. Magn. Mater. **405**, 17 (2016)
7. Sugimoto, S., Haga, K., Kagotani, T., Inomata, K.: J. Magn. Magn. Mater. **290–291**, 1188–1191 (2005)
8. Shafiu, S., Sozeri, H., Baykal, A.: J. Supercond Nov. Magn. **27**(6), 1593–1598 (2014)
9. Narang, S.B., Hudiara, I.S.: J. Ceram. Process. Res. **7**(2), 113 (2006)
10. Li, C.J., Wang, B., Wang, J.N.: J. Magn. Magn. Mater. **324**(7), 1305–1311 (2012)
11. Wang, Z., Zhou, Z., Zhang, W., Qian, H., Jin, M.: J. Supercond. Nov. Magn. **26**(12), 3501–3506 (2013)
12. Perez-Juache, T.J., Betancouurt, I., Palmare-Sanchez, S.A., Mirabal Garcia, M., Matutes Aquino, J.A., Guerrero-Serrano, A.L.: J. Supercond. Nov. Magn. **24**, 2325 (2011)
13. Singh, C., Narang, S.B., Hudiara, I.S., Raju, K.C.J., Sudheendran, K.: J. Ceram. Process. Res. **11**(6), 692–697 (2010)
14. Singh, C., Narang, S.B., Hudiara, I.S., Sudheendran, K., Raju, K.C.J.: J. Electroceram. **27**(3–4), 120–125 (2011)
15. Arora, A., Narang, S.B. J. Mater. Sci.: Mater. Electron. (2016). doi:10.1007/s10854-016-5092-2
16. Singh, A., Narang, S.B., Singh, K., Pandey, O.P., Kotnala, R.K.: J. Ceram. Process. Res. **11**(2), 241–249 (2010)
17. Ghasemi, A., Alam, R.S., Morisako, A.: Phys. B Condens. Matter **403**(18), 2987–2990 (2008)
18. Singh, C., Narang, S.B., Hudiara, I.S., Sudheendran, K., Raju, K.C.J.: J. Magn. Magn. Mater. **320**, 1657–1665 (2008)
19. Evans, B.J., Grandjean, F., Lilot, A.P., Vogel, R.H., Gerard, A.: J. Magn. Magn. Mater. **67**, 123–129 (1987)
20. Campbell, S.J., Wu, E., Jayasuriya, K.D., Kaczmarek, W.A.: IEEE Trans. Magn. **30**(2), 742–745 (1994)
21. Obradors, X., Collomb, A., Pernet, M., Samaras, D., Joubert, J.C.: J. Solid State Chem. **56**(2), 171–181 (1985)
22. Peng, Z., Fu, X., Ge, H., Fu, Z., Wang, C., Qi, L., Miao, H.: J. Magn. Magn. Mater. **323**(20), 2513–2518 (2011)
23. Alam, R.S., Tehrani, M.K., Moradi, M., Hosseinpour, E., Sharbati, A.: J. Magn. Magn. Mater. **323**(8), 1040–1043 (2011)
24. Choopani, S., Keyhan, N., Ghasemi, A., Sharbati, A., Alam, R.S.: Mater. Chem. Phys. **113**(2–3), 717–720 (2009)
25. Chang, S., Kangning, S., Pengfei, C.: J. Magn. Magn. Mater. **324**(5), 802–805 (2012)
26. Chen, N., Yang, K., Gu, M.: J. Alloys Compd. **490**(1–2), 609–612 (2010)
27. Ghasemi, A.: J. Magn. Magn. Mater. **324**(6), 1080–1083 (2012)
28. Guo, F., Ji, G., Xu, J., Zou, H., Gan, S., Xu, X.: J. Magn. Magn. Mater. **324**(6), 1209–1213 (2012)